論文 / 著書情報
Article / Book Information

Title	Centrifuge modeling of hybrid foundation to mitigate liquefaction-induced effects on shallow foundation resting on liquefiable ground
Authors	Ritesh Kumar, Masamichi Sawaishi, Kazuki Horikoshi, Akihiro Takahashi
Citation	Soils and Foundations, Vol. 59, Issue 6, pp. 2083-2098
Pub. date	2019, 12
DOI	http://dx.doi.org/10.1016/j.sandf.2019.11.002
Creative Commons	See next page.
Note	This file is author (final) version.

License

Title:

Centrifuge modeling of hybrid foundation to mitigate liquefaction-induced effects on shallow foundation resting on liquefiable ground

Authors:

Ritesh Kumar [a], Masamichi Sawaishi [b], Kazuki Horikoshi [a], Akihiro Takahashi [a, *]

[*]**Corresponding author:**

Akihiro Takahashi

Email: takahashi.a.al@m.titech.ac.jp

Tel: +81-(0)3-5734-2593 Fax: +81-(0)3-5734-3577

Address:

[a] Department of Civil and Environmental Engineering

Tokyo Institute of Technology, Japan

[b] Nippon Steel Corporation

Tokyo, Japan

Soils and Foundations, 59(6), 2083-2098, 2019

Original URL: https://doi.org/10.1016/j.sandf.2019.11.002

Abstract

A hybrid foundation is developed in this study to mitigate the liquefaction-induced effects on shallow foundations. The proposed hybrid foundation is a combination of a gravel drainage system and friction steel piles with spiral blades, framed under the footing. The motivation behind having a gravel drainage system, as an integral part of the hybrid foundation, is its ability to improve the liquefaction resistance of the ground in the most economical way. However, case histories and the development of recent research have highlighted that gravel drainage systems have exhibited poor performances and could not prevent ground liquefaction during strong ground motion. To counteract these shortcomings, friction steel piles are provided which are supposed to yield frictional resistance during earthquakes and are presumed to minimize the rocking/tilting behavior of the foundation-structure system even if the ground undergoes liquefaction. The evolution of excess pore water pressure, specifically in the vicinity of the foundation-structure system, dominatingly influences the settlement mechanism of shallow foundations. Centrifuge test results show that the presence of gravel drainage can minimize the post-liquefaction settlement of shallow foundations through the rapid dissipation of excess pore water pressure. Moreover, friction piles are able to minimize the tilting/differential settlement of shallow foundations. It is found that the proposed hybrid foundation provides the desired function of reducing the overall liquefaction-induced effects on shallow foundations resting on liquefiable grounds.

Keywords

Dynamic centrifuge tests, friction piles, gravel drainage system, hybrid foundation, liquefaction, shallow foundation

1. Introduction

Numerous instances of damage to the built environment on shallow foundations, such as settlement, tilting, and sinking due to liquefaction, have been witnessed all over the world during many past earthquakes. In the 1964 Niigata (Japan) and 1990 Luzon (Philippines) Earthquakes, most of the damaged buildings were two to four stories in height and founded on shallow foundations and relatively thick and uniform deposits of clean sand (Liu and Dobry, 1997, Olarte et al., 2017). In the 1999 Kocaeli (Turkey) Earthquake, many of the damaged structures were surprisingly influenced by the liquefaction of thin deposits of silt and silty sand (Bray et al., 2000, Bird and Bommer, 2004). Many researchers (Nakai and Sekiguchi, 2011, Bhattacharya et al., 2011, Tokimatsu and Katsumata, 2012, Yamaguchi et al., 2012) have described the role of liquefaction in the damage of buildings, specifically referring to the liquefaction of reclaimed land during the 2011 Tohoku Earthquake in Japan.

The overall deformation mechanism of a shallow foundation resting on a liquefiable ground is a complex phenomenon. It is presumed to be affected by several factors, e.g., induced cyclic stress, foundation configuration, ground conditions, shear-induced deformation, development of excess pore water pressure (EPWP), localized drainage, post-liquefaction reconsolidation, void re-distribution, and inertial and kinematic interaction within the soil-foundation-structure system (Dashti et al., 2009). The well-known procedures for evaluating the liquefaction-induced settlement in the free-field by Tokimatsu and Seed, 1987, Ishihara and Yoshimine, 1992 do not incorporate the combined effects of shear and volume change-induced building settlement due to cyclic soil softening/hardening under static and dynamic loading. Many researchers (Yoshimi, 1997, Liu and Dobry, 1997, Sancio et al.,

2004) have found that the foundation width and the height/width ratio are two of the governing factors which influence the building settlement/tilt along with the bearing failure. It is suggested that 3D drainage affects the overall settlement behavior of shallow foundations as partial drainage is shown to occur simultaneously with the generation of EPWP because of the migration of pore fluid towards the top surface (Liu and Dobry, 1997). However, a well-accepted settlement mechanism, due to drainage, has not yet been established.

The total settlement of a shallow foundation during a dynamic event can be divided into two phases; i.e., co-shaking settlement and post-shaking settlement. The shear-induced settlement mechanism dominates the co-shaking settlement behavior of a shallow foundation, as has been presented in many studies (Elgamal et al., 1989, Dobry and Liu, 1992, Kokusho, 1999). The post-shaking settlement behavior of a shallow foundation is believed to be affected by changes in density, the development of volumetric strain, and the permeability of the ground (Ishihara and Yoshimine, 1992, Liu and Dobry, 1997, Shamoto et al., 1998, Zhang and Wang, 2012, Kumar et al., 2019).

Hausler and Sitar (2001) studied more than 90 case histories on the performance of improved sites from 14 earthquakes in Japan, Taiwan, Turkey, and the United States. They found that about 10 percent of the surveyed sites required significant post-earthquake remediation or demolition because of liquefaction. This emphasizes that even after ground improvement, the effects of liquefaction cannot be entirely avoided. Mitchell et al. (1995) explained the use of different soil mitigation methodologies to countermeasure the liquefaction-induced effects. A few other documented studies by Mitchell, 1981, Schaefer et al., 1997 describe technical specifications, limitations, applicability, and the design

procedure of liquefaction mitigation methodologies.

The hybrid foundation proposed here is a combination of the gravel drainage system and friction piles having spiral blades devised under the footing as a hybrid mitigation technique against the liquefaction-induced effects on shallow foundations. Liquefaction mitigation by gravel drainage piles is one of the pronounced techniques used to help quickly dissipate the EPWP generated during an earthquake, eventually increasing the liquefaction resistance of the liquefiable ground (Seed and Booker, 1977, Priebe, 1989, Baez and Martin, 1993, Adalier et al., 2003). The satisfactory performance of gravel drainage against small magnitude earthquakes has been corroborated by physical model tests and field studies carried out by many researchers (Priebe, 1989, Baez and Martin, 1993, Adalier et al., 2003, Brennan and Madabhushi, 2006). However, during a moderate or strong earthquake, the build-up of EPWP due to shaking may exceed the capacity of the gravel drainage system; and apparently, the foundation ground may be liquefied. The large dissipation rate of EPWP after the liquefaction, due to the presence of gravel drains, may adversely increase the post-liquefaction settlement of the foundation and associated structure.

To overcome the limitations of gravel drainage and to minimize the differential settlement of shallow foundations in the case of liquefaction occurring within the ground, friction piles with spiral blades are proposed under the footing as an integral part of the hybrid foundation. It should be noted that the proposed hybrid foundation has been tested for temporary structures, such as the Buffer Tank and Flare Stack at an industrial process plant. After the lifespan of the structure, it is planned that the hybrid foundation will be re-used for a different structure by keeping the gravel drains and re-installing

the friction piles. For this reason, the piles are not fixed to the footing, i.e., the piles and the footing have a certain clear spacing between them to allow for relative vertical movement and to limit the tilting of the footing. The diameter of the footing hole through which the friction pile passes is maintained at 1.25 times the outer diameter of the friction piles. The ease of the centrifuge modeling for Models 4–6 and the friction pile installation sequence are also considered when selecting the minimum clear spacing between the friction piles and the footing. The friction piles are supposed to yield frictional resistance during an earthquake and are presumed to minimize the rocking/tilting behavior of the foundation structure system. The stress of the foundation-structure system is supposed to be transferred through the ground (not through the friction piles); and hence, a clear marginal spacing is kept between the friction piles and the footing to avoid subsidence below the footing during the shaking.

2. Development scheme

The development of the hybrid foundation is carried out with the help of a physical model using the centrifuge lab facility at the Tokyo Institute of Technology. The presented research is conducted in three phases. All the model configurations are shown in Fig. 1. In the first phase, an attempt is made to understand the behavior of a shallow foundation resting on a liquefiable ground (using Model 1) during strong ground motion. In the second phase, the performance of the gravel drainage system and the friction piles are investigated. Three types of model tests are performed (using Models 2–4) in which two model tests consist of the gravel drainage system with different drainage capacities, and

one model test consists of only friction piles as the liquefaction countermeasure. In the third stage, the performance of the hybrid foundation is investigated through two model tests (using Models 5 and 6). Each model test consists of friction piles and a gravel drainage system of different drainage capacities as individually investigated in the second phase.

The performance of the hybrid foundation is assessed based on the generation and dissipation of excess pore water pressure (EPWP), the settlement and tilting of the shallow foundation, the behavior of the model ground, the seismic demand on the superstructures, the bending moment and the axial force exerted on the friction piles, and the overall soil-structure-interaction. The suitability and the effectiveness of the hybrid foundation are evaluated against temporary structures, such as the Buffer Tank (BT) and Flare Stack (FS), imposing average bearing pressures of 51.2 kPa and 71.2 kPa, respectively, 0.8 m below the surface of the model ground in the prototype scale. The two structures are mounted on different shallow foundations. Dynamic centrifuge tests are carried out at the Tokyo Tech Mark III centrifuge facility (Takemura et al., 1999) having a radius of 2.45 m and a centrifugal acceleration of 40g (N = 40; scaling law is tabulated in Table 1). The presented centrifuge tests simulated the prototype saturated soil deposit with a depth of 10 m and a water table 1.8 m below the top surface. The heights of prototype targeted structures BT and FS are 15 m and 32 m, respectively, and the mass is distributed along the height. In the model scale, the height of both BT and FS (after scaling down for N = 40) turns out to be quite disproportionate as per the laminar container size. To ensure the fundamental design periods of BT and FS (0.4 s and 0.5 s, respectively), and to adjust the center of gravity of the centrifuge model, masses are lumped at the top of both BT and FS. This

improvisation reduces the heights of BT and FS by 50.10% and 56.25%, respectively. The configurations of the model foundation and the structure system are tabulated in Table 2.

3. Centrifuge testing program

A flexible laminar container with inner dimensions of 600 × 250 × 438 mm (model scale) in length, width, and height, respectively, is used to frame the models. The laminar box is composed of many aluminum rectangular alloy rings which allow its movement along with that of the soil mass, creating a flexible boundary and establishing uniform dynamic shear stresses within the model ground during the dynamic excitation. The model ground is prepared using Toyoura sand having a target relative density of 50% by the air pluviation method using a sand hopper. The sand hopper is calibrated in terms of the falling height and the pouring rate of the Toyoura sand to ensure the consistency of the relative densities for the different model grounds (Models 1–6). The sides of the laminar box are covered with polyethylene sheets to secure water tightness and to prevent any sand particles from jamming the alloy rings. Then, the Toyoura sand (properties are shown in Table 3) is poured into the box with the help of the sand hopper which is manually moved back and forth to achieve a uniform level ground at the calibrated falling height and pouring rate. During the model ground preparation, many transducers are carefully placed at the desirable locations, as shown in Fig. 2 (positions are tabulated in Table 4). The initial vertical effective stress is calculated by subtracting the pore water pressure from the total stress. Boussinesq's method is used to calculate the vertical stress due to the foundation-structure at the required depths; the vertical stress method is further used to estimate the vertical effective stresses tabulated in Table 4.

The guide frames are prepared to make the gravel drainage system presented in Fig. 3. The frames are kept at desirable locations (under both BT and FS) while preparing the model ground. Initially, the gravel drain casings are covered with tape while the Toyoura sand is being poured into the box. The guide frame has large enough openings for the Toyoura sand to pass through the frame and to form a uniform model ground in the vicinity of the gravel drains. After achieving the required level of the model ground with the Toyoura sand, Silica sand no. 3 is carefully poured inside all the gravel drain casings. Then, the guide frames are taken out of the model ground with due care to avoid any possible disturbance or densification within the model ground. It should be noted that the length of the gravel drain casings attached to the guide plates are kept 10 mm (in model scale) longer than the required length of the gravel drains in the model ground. The reason for this is to form a 10-mm deep (0.4 m in prototype scale) gravel mat over the group of gravel drain piles. From Fig. 3, a little overflow of Silica sand no. 3 is evident which, in turn, is used to form the gravel mat with a thickness of 10 mm (in model scale). By adding Silica sand no. 3, the gravel mat is formed with due care to avoid any densification around the gravel drains. After finishing the model ground preparation, the friction piles (properties are shown in Table 3) are inserted in the model ground by means of screw driving. Care should be taken when inserting the friction piles to avoid/minimize any possible disturbance or densification of the model ground.

The model ground is saturated with viscous fluid, i.e., a mixture of water and 2.0% Hydroxypropylmethylcellulose solution (Metolose by Shin-Etsu Chemical Co., Ltd.; grade 60SH-50) by weight of water, to achieve a viscosity about 50 times that of water. This solution is used to ensure

the compatibility of the prototype permeability of the soil for setting up the affinity between the dynamic and the diffusion scaling laws (Schofield, 1981). The saturation within the model ground is achieved by dripping the de-aired Metolose solution slowly from the top of the container under a vacuum of 760 mmHg over the sponges at the surface of the model ground. The dripped solution slowly moves downward and saturates the model ground uniformly. The saturation is continued until the water table (Metolose solution table) reaches the top surface of the model ground. The saturation process for all the models takes approximately 55 h to complete. After the saturation, the superstructures are mounted over the footings (more details on the model ground preparation and the saturation process can be found in Kumar et al., 2019). The relative densities and degrees of saturation (at 1 g) for all the models, Models 1–6, are tabulated in Table 5. Due care is taken to estimate the degrees of saturation for all the model grounds using the mass, volume, and density relationships. However, it is worth noting that certain errors still occur, as mentioned by Kutter (2013).

After the model preparation, the instrumented model is placed in the centrifuge and spun at the centrifugal acceleration of 40g. Then, the Metolose solution is drained out using the pre-installed standpipes and a valve at the base of the container to bring the water table down to a depth of 1.8 m (in prototype scale) at 40g. For the realistic seismic response of a liquefiable model ground, the simulated motion in the centrifuge should reasonably reproduce the full range of frequencies present in the recorded earthquake motion. All the models (Models 1–6) are tested under the earthquake ground motion that was recorded at Hachinohe Port in the 1968 Tokachi-Oki Earthquake (NS component). Before applying the Tokachi-Oki ground motion, the models are subjected to white noise to evaluate

the dynamic characteristics of the system.

Fig. 4 shows the prescribed and the actual input Tokachi-Oki ground motions in the centrifuge for Models 1–6. Only the acceleration time histories of Model 1 are shown for the sake of brevity. All the input motions are presented after having baseline correction and filtering. Filtering is performed in the frequency domain using the bandpass Butterworth filter with corner frequencies of 0.3 Hz and 10 Hz, respectively. The actual input Tokachi-Oki ground motions for Models 1–6 are in reasonably good agreement with the prescribed Tokachi-Oki ground motions. The repeatability of the input motions, both in frequency and time domain, is satisfactory. Fig. 4 shows that the Arias intensity of the actual input motion is large in the case of Model 6 in comparison with that in Models 1–5. Although due care is taken during all the experiments, this kind of inconsistency is inevitable when simulating ground motion in dynamic centrifuge experiments.

4. Design of gravel drainage system

Design charts reported by Seed and Booker (1977) in their seminal work and the revised guidelines presented by Bouckovalas et al. (2006) are used to design the gravel drainage system for Models 2 and 3 (shown in Fig. 1). Many parameters, e.g., replacement area, target excess pore water pressure ratio, earthquake intensity, reported case histories, and installation methodology of gravel drains, are considered when designing the gravel drainage system. Design specifications for both gravel drainage Types 1 and 2 are tabulated in Table 6. Liquefaction resistance curves for saturated Toyoura sand with a relative density of 50% ± 5% for different confining pressure levels are obtained using the laboratory

test results of Chiaro et al. (2012). Based on Seed and Booker (1977), it is found that the Tokachi-Oki ground motions can be considered as representing a medium EQ to a strong EQ (as specified in Table 6) for Models 1–6. It is evident that gravel drainage Type 1 does not satisfy the design guidelines because the clear spacing between the drains is more than the maximum allowable spacing for a medium EQ to a strong EQ. Initially, it is hypothesized that gravel drainage system Type 1 could render the targeted performance of the hybrid foundation along with friction piles having spiral blades. However, the centrifuge test results for Model 2 demonstrated the inefficiency of gravel drainage system Type 1, in terms of both the generation and dissipation of EPWP, which will be elaborated in subsequent subsections. Based on the performance of gravel drainage system Type 1, the redesign of the gravel drainage system is done, and new gravel drainage system Type 2 is tested on Model 3 which satisfies the design guidelines tabulated in Table 6. In addition, in order to provide significant drainage for the developed EPWP to dissipate, the focus is placed on the shear-induced and post-liquefaction/shaking settlement, due to the presence of gravel drains, which alter the stresses and strains applied to the improved ground, as highlighted by Priebe, 1989, Baez and Martin, 1993, and Adalier et al. (2003).

5. Centrifuge test results

5.1 Liquefaction-induced effects on shallow foundation

An attempt is made to understand the behavior of a shallow foundation resting on a liquefiable ground (using Model 1) during strong ground motion. All the test results shown in and after this subsection

are in prototype scale unless otherwise mentioned. The evolution of excess pore water pressure (EPWP) plays a vital role in the manifestation of liquefaction during a dynamic event. Fig. 5 depicts the EPWP generation and dissipation trends within the ground during the Tokachi-Oki ground motion. Soils at certain depths undergo the liquefaction state if the excess pore water pressure ratio (r_u), which is calculated by dividing the generated EPWP by the initial vertical effective stress at the respective depth, reaches one. It is evident from Fig. 5 that the ground liquefies at Level 3 (different levels in the model ground are shown in Fig. 2) under both FS (at P2) and BT (at P4). However, at P3, the maximum magnitude of the EPWP does not reach the liquefaction state (r_u = 1 line). The ground exhibits the liquefaction state at Level 4 under BT (at P7) and along the model centerline (at P6); however, the time history of P5 shows that the ground does not liquefy under FS at Level 4. The induced cyclic stress ratio under FS during the shaking is relatively small as the initial vertical effective stress at P5 (see Table 4) is significantly large in comparison to that at either P6 or P7, which prevents the liquefaction state from being achieved at Level 4 under FS. Overall, the whole ground either liquefied or nearly reached the liquefaction state during the Tokachi-Oki ground motion except in the vicinity of the FS footing. Soon after the shaking terminates, the EPWP starts dissipating at Level 3 (at P2, P3, and P4). It is apparent that at shallower depths (at Levels 4 and 5), the pore pressure does not show any traces of dissipation, even after shaking, until approximately 400 s. The reason for the delayed dissipation of the EPWP at shallower depths is the availability of the migrated pore fluid from deeper locations even after shaking for quite a long time. Drainage is only possible through the top surface of the ground; and hence, a sufficient upward hydraulic gradient is established during the shaking. The EPWP at

shallower depths starts dissipating as soon as the migrated pore fluids recede from the deeper portions. All the graphs in Fig. 5 show the marginal magnitude of the residual EPWP in the dissipation phase (e.g., at 2000 s). This is associated with the fact that the pore pressure transducers (PPTs) undergo a marginal settlement during the Tokachi-Oki ground motion along with changes in the overall void ratio (probably decreases) due to ground deformation and a slight rise in the water table.

Four laser displacement transducers (LDTs), shown in Fig. 2, are employed to record the settlement time histories of the BT (using LDT1 and 2) and FS (using LDT3 and 4) footings, and the results are plotted in Fig. 6. It is evident that both the BT and FS footings undergo significant settlement during the Tokachi-Oki ground motion. The foundations begin to settle immediately after the shaking starts and continue settling even after the shaking ceases. Relatively large differential settlement of the FS footing is observed in comparison with that of BT footing. Initially, it was hypothesized that the taller structure (FS) might show traces of rocking motion. However, no evidence of rocking motion is seen in Fig. 6 for either the BT or the FS foundation-structure system even though they both undergo excessive settlement during the dynamic event.

The assumption of the undrained condition is not valid during the dynamic event as partial drainage starts to occur through the top surface of the ground as soon as the shaking begins. The shear strength of soil in the vicinity of the foundation begins to mobilize because of the generation of EPWP (reduction in mean vertical effective stress); and hence, shear-induced settlement during shaking is apparent. The excessive settlement of both BT and FS, which cumulatively take place during both co-shaking and post-shaking periods, demonstrates that a shallow foundation resting on a liquefiable

ground is prone to severe liquefaction-induced deformation during an earthquake. Shear-induced deformation is the governing factor of settlement during shaking (co-shaking settlement from t = 10 to 74 s), and it can be seen from Fig. 7 that the overall vertical settlement of FS is almost twice that of BT. A significant amount of post-shaking settlement of both BT and FS is apparent from Fig. 7.

Fig. 8 shows the recorded acceleration time histories within the ground and at the foundation-structure system for Model 1 during the Tokachi-Oki ground motion. All the observed acceleration records at Levels 2–5 show significant de-amplification (attenuation) in acceleration amplitude after 20 s (10 s from the beginning of shaking); the acceleration records for Levels 1 and 5 are shown in Fig. 8. The reason for this considerable de-amplification is soil softening due to the mobilization of shear strength during the seismic event. This is also attributed to the development of the liquefaction state; specifically, at shallower depths, except in the vicinity of the footings. The acceleration transducers at the foundation-structure systems (A6-A8) show amplified traces of acceleration records from 10 to 15 s (initial 5 s of shaking). Later on, however, they also exhibit de-amplified records because of a lower transferred seismic demand brought about by the liquefaction caused during the shaking within the ground.

5.2 Effectiveness of gravel drains

The performance of the gravel drainage systems (Types 1 and 2 as described in Table 6) is investigated for Models 2 and 3. The excess pore water pressure (EPWP) time histories of the different pore pressure transducers (PPTs) for Models 2 and 3 are presented and compared with the EPWP time histories of the respective PPTs for Model 1 in Fig. 9. It is evident from this figure that the dissipation rate of the

EPWP increases in accordance with the gravel drainage capacity. It should be noted that the drainage capacity of the gravel drainage system in Model 3 is more than that in Model 2. The larger the drainage capacity, the quicker the dissipation of the EPWP, as was designed. For instance, at Level 3 (at P2, P3, and P4), the EPWP takes approximately 1000 s to dissipate in the case of Model 1 (no gravel drains), whereas the EPWP dissipates within 400 s in the case of Model 3. The foremost reason for the inefficiency of gravel drainage system Type 1 in the case of Model 2 is the lower drainage capacity. The targeted excess pore water pressure ratio (described in Table 6) at the liquefied zone within the ground cannot be achieved even in the case of Model 3 as the maximum magnitude of the EPWP at all the PPTs (P1-P10), for Models 2 and 3, is almost similar to the maximum magnitude observed in Model 1 for the respective PPTs. Surprisingly, the maximum EPWP at P9 and P10 in the case of Model 2 is more than that observed in the case of Model 1. This might be associated with the non-uniformity of the model ground and possible densification due to the presence of gravel drains or the relatively deeper positioning of the PPTs. Although the capacity of gravel drainage system Type 1 is not sufficient to dissipate the EPWP, relatively larger permeability of the gravel drains might lead to the flow of water from deeper portions to shallower portions with more ease, resulting in large EPWP at the shallower portions in the case of Model 2.

The settlement time histories of both the BT and FS foundations in Models 2 and 3 are presented and compared with the respective settlement time histories of Model 1 in Fig. 10 The influence of gravel drainage system Type 1 (Model 2) on the settlement mitigation is not significant. However, the overall settlement in the case of Model 3 is less in comparison with that of Models 1 and 2 due to the

presence of sufficient gravel drainage capacity. Considerable differential settlement for BT occurs in the case of Model 3 because of the unusual change in the initial condition before dynamic excitation. While spinning the centrifuge up to 40g, the BT foundation experiences a significant amount of differential settlement probably because of the non-uniformity of the model ground. This uneven settlement of the BT foundation before shaking exaggerates the differential settlement during the Tokachi-Oki ground motion, as shown in Fig. 10.

Fig. 11 shows the average settlement of the foundations during both co-shaking and post-shaking phases. In the case of Model 1, the foundations undergo excessive settlement during both co-shaking and post-shaking phases of the dynamic event. However, in the case of Models 2 and 3, the significant settlement of both BT and FS foundations occurs during the co-shaking phase. Fig. 11 also shows that the effect of the post-liquefaction/shaking reconsolidation mechanism seems to be overshadowed by the presence of the gravel drainage system which helps to reduce the total settlement of the shallow foundation.

An attempt is made to estimate the pore fluid flow (vectors with total hydraulic head and resultant direction) during the Tokachi-Oki ground motion at different time intervals. As the EPWP was only recorded at nine locations during the experiment (Fig. 2), linear interpolation of the EPWP is done to estimate the pore fluid flow at several locations within the ground. Initially, the hydraulic gradient field is estimated by the pore pressure distribution, and then the flow direction is estimated by the hydraulic gradient field. The following assumptions are made to obtain the qualitative pore fluid flow within the ground. The EPWP evolution at lengths of 0 m and 24 m is assumed to be same as that along the model

centerline. This assumption ignores the boundary effects of the laminar container on the evolution of pore water pressure at the boundaries. A linear interpolation of the EPWP at the non-measured locations might not be accurate at shallower depths (in the vicinity of the BT and FS footings to be specific), because of the different confining pressure levels. However, the above-mentioned effects can be ignored for the overall qualitative representation of the pore fluid flow.

The pore fluid flow within the ground in the case of Model 1 is shown in Fig. 12 during the Tokachi-Oki ground motion. As mentioned in Section 5.1, the dissipation of pore pressure is only permitted from the surface of the model ground. Hence, the flow of pore fluid is always dominatingly upward, even after the shaking ceases, and then continues until the pore fluid pressure reaches the equilibrium state throughout the ground (Zeybek and Madabhushi, 2017), which is also apparent from Fig. 12. In the case of Model 3, the drainage effects of the gravel drainage system are apparent as the radial flow (towards the gravel drainage zone) is set, as shown in Fig. 12. However, at shallower depths, as the pore fluid tends to flow to the horizontal drainage boundary at the groundwater level, the pore fluid flow is almost vertical. In addition, the influence of the gravel drains along the model centerline seems to be negligible as the fluid flows for Models 1 and 3 are very much alike.

5.3 Effectiveness of friction piles

Model 4 (see Fig. 1) is used to investigate the effectiveness of the friction piles. The excess pore water pressure (EPWP) evolution for Model 4 at different pore pressure transducers (PPTs) is found to be mostly in accordance with that for Model 1 as the ground conditions of the two models are alike. Fig. 13 shows the settlement time histories of both BT and FS foundations in Models 1 and 4. It is evident

that the presence of friction piles reduces the overall settlement of shallow foundations significantly for both BT and FS. However, the friction piles are not able to restrict the post-shaking settlement of the foundation, which is the desired function, as the piles are not fixed to the footings, although the post-shaking settlement rate decreases for Model 4 in comparison to that for Model 1. Unfortunately, LDT4 does not work in the case of Model 4 and the differential settlement of FS cannot be measured. However, a visual inspection after the experiment indicates less differential settlement of the FS foundation in the case of Model 4 in comparison to that of Model 1.

During the centrifuge experiments, two dominating mechanisms, i.e., the inertial interaction between the foundation-structure system and the kinematic interaction due to the friction piles and the relative model ground movement, govern the overall soil-structure interaction phenomena. The seismic load exerted on the friction piles is recorded in terms of the bending moment (BM) and the axial force (AF) at several locations, as shown in Fig. 1. The seismic demand on the superstructure is further deduced using the recorded acceleration time histories at the foundation-structure system. Fig. 14 shows the bending moment exerted on the BT and FS friction piles during the Tokachi-Oki ground motion. The bending moment time histories show that the friction piles experience a significant bending moment for both BT and FS during the shaking. The residual bending moment in the post-shaking phase is also apparent. The bending moment exerted on the friction piles substantially depends on the inertial force/stress due to the foundation-structure mass and the relative pile and soil movement during the dynamic event. Unfortunately, the precise relative movement of the friction piles and the surrounding soil cannot be evaluated due to the limited number of friction pile sensors and the absence

of acceleration transducers under the centerline of the BT and FS footings.

Friction piles, as an integral part of the hybrid foundation, are provided presuming that they will help to avoid/minimize the tilting and rocking motion of both BT and FS. However, experimental results show that the rocking behavior is not dominating even in the case of the taller structure (FS), as discussed in Section 5.1. Axial force sensors (AF1 and AF2) are used to examine the load taken by the piles, as shown in Fig. 1. The maximum recorded axial force in the case of FS is found to be 3-6 times more than the axial force in the case of BT. One of the main purposes of providing the free connection between the footing and the friction piles is to avoid any subsidence below the footing, i.e., the formation of gaps between the footing and the soil below it, during the shaking. Subsidence commonly takes place under the footing if the piles are fixedly connected with it. In that case, significant stress from the foundation structure system is transferred through the piles. Large exerted AF in the case of the FS footing indicates that the FS piles experience significant fixity with the footing, although the friction piles (4 mm in diameter at the pile head in the model scale) pass through the corners of the footings with a clear spacing of 0.5 mm (in the model scale). In other words, theoretically, the footing and the piles should exhibit a free connection; in fact, this did happen to a great extent in the case of the BT footing. However, due to the large thickness of the FS footing, the semi/fully rigid connection between the FS footing and the piles is inevitable. In this case, the transferred axial force through the piles and BM at the pile heads largely depends upon the uncertain fixity condition between the pile heads and the footing.

5.4 Performance of hybrid foundation

In the final stage, two centrifuge tests (Models 5 and 6) are carried out to traverse the performance of the proposed hybrid foundation (having both gravel drainage and friction piles) to mitigate the liquefaction-induced effects on a shallow foundation resting on a liquefiable ground. Initially, the liquefiable ground is treated with gravel drainage system Type 1 and friction piles in Model 5; then, the liquefiable ground is treated with gravel drainage system Type 2 and friction piles in Model 6, as shown in Fig. 1. The independent effects of gravel drainage system Types 1 and 2, and the friction piles, in mitigating the liquefaction effects, are evaluated and presented in 5.2 Effectiveness of gravel drains, 5.3 Effectiveness of friction piles, respectively.

The excess pore water pressure (EPWP) time histories for Models 5 and 6 are presented and compared with the EPWP time histories for Model 1 in Fig. 15. It is evident from this figure that the dissipation rate of the EPWP increases because of the gravel drainage system. It should be noted that the drainage capacity of the gravel drainage system is greater in the case of Model 6 than Model 5, as assigned. The larger the drainage capacity, the faster the dissipation of the EPWP. For instance, at Level 3 (at P2, P3, and P4), the EPWP takes approximately 1000 s to dissipate in the case of Model 1 (no gravel drains), whereas the EPWP dissipates within 600 s in the case of Model 6. However, in the case of Model 5 (having gravel drainage system Type 1), the dissipation rate of the EPWP is almost similar to that of Model 1. The reason for the inefficiency of gravel drainage system Type 1 in the case of Model 5 is the lower drainage capacity, as discussed in Section 5.2. The maximum magnitude of the EPWP at Level 4 (at P5, P6, and P7) in Model 6 is significantly less than that in Model 1, as shown in

Fig. 15. However, Fig. 9 depicts that the maximum magnitude of the EPWP in the case of Model 3 (having the same drainage system as that in Model 6) at Level 4 (at P5, P6, and P7) is almost the same as that in the case of Model 1, although Model 6 has friction piles which have a negligible effect on the evolution of the EPWP, as explained in Section 5.3. The reason for this is the shallower positioning of the PPTs at Level 4. The positioning of the PPTs at Level 4 are back-calculated using the hydrostatic pressure at 40 g (before the shaking), and it is found that the PPTs are placed in positions approximately 8–9 mm (in model scale) shallower than the required depth. The targeted excess pore water pressure ratio (described in Table 6) at the liquefied zone within the ground cannot be achieved in either Model 5 or Model 6 (except at Level 4 in the case of Model 6) as the maximum magnitudes of the EPWP for both Models 5 and 6 are almost similar to the one observed for Model 1. It should be noted that the gravel drainage system, in both Models 5 and 6, cannot prevent the liquefaction of the model ground.

The settlement time histories of both BT and FS foundations in Models 5 and 6 are presented and compared with the respective settlement time histories of Model 1 in Fig. 16. It is evident that the overall settlement of both BT and FS is significantly less in the case of Model 6 than in the cases of Models 1 and 5. Gravel drainage system Type 2 can mitigate the post-shaking settlement, while the friction piles contribute to minimizing the co-shaking deformation of both footings. To examine the combined influence of the gravel drainage system and the friction piles, the cumulative settlement progression of the footings at different time intervals is shown in Fig. 17 for Models 1 (no treatment), 3 (gravel drainage Type 2 only), 4 (friction piles only), and 6 (both gravel drainage Type 2 and friction piles). It is evident that the presence of gravel drainage minimizes the post-shaking settlement (after

100 s) in Models 3 and 6. Although the settlement during shaking is small in the case of Model 4, in comparison to that of Models 1 and 3, a comparatively large amount of settlement occurred after shaking in the case of Model 4. The combined effects of both the friction piles and gravel drainage Type 2 are evident in the case of Model 6 as the settlement occurring in all time intervals is significantly less than that occurring in the cases of Models 1, 3, and 4.

6. Summary and conclusions

A unique hybrid foundation has been proposed to mitigate the liquefaction-induced effects on a shallow foundation. The proposed hybrid foundation is a combination of gravel drainage and friction piles with spiral blades. The intended purpose of providing the gravel drainage was to mitigate the liquefaction-induced effects through the rapid dissipation of excess pore water pressure (EPWP). Moreover, the friction piles were presumed to minimize the excessive settlement/tilting of the foundation system during strong ground motion. The efficacy of the hybrid foundation in mitigating the liquefaction-induced effects on the shallow foundation was investigated using a series of dynamic centrifuge experiments. The research was carried out in three phases. In the first phase, an attempt was made to understand the behavior of a shallow foundation on a liquefiable ground during Tokachi-Oki ground motion. In the second phase, the performance of the gravel drainage system and the friction piles was evaluated. Three types of model tests were performed for this purpose in which two model tests consisted of the gravel drainage system with different drainage capacities, and one model test consisted of only friction piles. In the third stage, the performance of the hybrid foundation was

investigated using two model tests. Each model test consisted of the friction piles and the gravel drainage system with different drainage capacities as individually investigated in the second phase.

It was found that a shallow foundation resting on a liquefiable ground is prone to excessive settlement. Shear and volume change-induced deformation were seen to dominate the overall settlement of the shallow foundation. Treating the ground with the gravel drainage system was found to be useful in mitigating the liquefaction-induced deformation. The presence of gravel drainage increased the dissipation rate (through the radial flow towards the gravel drainage zone) of the generated EPWP and decreased the post-shaking settlement. The centrifuge test results showed that the friction piles having spiral blades at the bottom served as an excellent means of frictional resistance against the settlement of the shallow foundation and reduced the overall deformation of the shallow foundation significantly through combined inertial and kinematic interaction with the foundation-superstructure and the model ground. Overall, the hybrid foundation performed as expected in mitigating the liquefaction-induced effects on the shallow foundation during strong ground motion.

Acknowledgments

The work presented in this paper is part of a collaborative research of Nippon Steel & Sumikin Engineering. The first author is sincerely grateful for the support provided by the Monbukagakusho (Ministry of Education, Culture, Sports, Science, and Technology) scholarship for graduate students. The authors are also indebted to Mr. Sakae Seki, lab technician, Department of Civil and Environmental Engineering, Tokyo Institute of Technology, for his tremendous contribution to the successful completion of the centrifuge experiments.

References

Adalier, K., Elgamal, A., Meneses, J., Baez, J. I., 2003. Stone columns as liquefaction countermeasure in non-plastic silty soils. Soil Dynamics and Earthquake Engineering 23 (7), 571-584. *https://doi.org/10.1016/S0267-7261(03)00070-8*

Baez, J. I., Martin, G. R., 1993. Advances in the design of vibro systems for the improvement of liquefaction resistance. International Symposium for Ground Improvement, 1-16.

Bhattacharya, S., Hyodo, M., Goda, K., Tazoh, T., Taylor, C. A., 2011. Liquefaction of soil in the Tokyo Bay area from the 2011 Tohoku (Japan) earthquake. Soil Dynamics and Earthquake Engineering 31 (11), 1618-1628. *https://doi.org/10.1016/j.soildyn.2011.06.006*

Bird, J. F., Bommer, J. J., 2004. Earthquake losses due to ground failure. Engineering geology 75 (2), 147-179. *https://doi.org/10.1016/j.enggeo.2004.05.006*

Bouckovalas, G. D., Papadimitriou, A. G., Kondis, A., Bakas, G. J., 2006. Equivalent-uniform soil model for the seismic response analysis of sites improved with inclusions. In Proc., 6th European Conference on Numerical Methods in Geotechnical Engineering, Taylor & Francis, London, 801-807.

Bray, J. D., Stewart, J. P., Baturay, M. B., Durgunoglu, T., Onalp, A., Sancio, R. B., Barka, A., 2000. Damage patterns and foundation performance in Adapazari. Earthquake Spectra 16 (1), 163-189. *https://doi.org/10.1193/1.1586152*

Brennan, A. J., Madabhushi, S. P. G. 2006. Liquefaction remediation by vertical drains with varying penetration depths. Soil Dynamics and Earthquake Engineering, 26 (5), 469-475. *https://doi.org/10.1016/j.soildyn.2005.10.001*

Chiaro, G., Koseki, J., Sato, T. 2012. Effects of initial static shear on liquefaction and large deformation properties of loose saturated Toyoura sand in undrained cyclic torsional shear tests. Soils and Foundations, 52(3), 498-510. *https://doi.org/10.1016/j.sandf.2012.05.008*

Dashti, S., Bray, J. D., Pestana, J. M., Riemer, M., Wilson, D., 2009. Mechanisms of seismically induced settlement of buildings with shallow foundations on liquefiable soil. Journal of geotechnical and geo-environmental engineering 136 (1), 151-164. *https://doi.org/10.1061/(ASCE)GT.1943-5606.0000179*

Dobry, R., Liu, L., 1992. Centrifuge modeling of soil liquefaction. In Proc., 10th World Conf. on Earthquake Engineering, 6801-6809.

Elgamal, A. W., Dobry, R., Adalier, K., 1989. Small scale shaking table tests of saturated layered sand-silt deposits. In 2nd US-Japan Workshop on Soil Liquefaction Rep. No. 89, 32, 233-245.

Hausler, E. A., Sitar, N., 2001. Performance of soil improvement techniques in earthquakes.

Ishihara, K., Yoshimine, M., 1992. Evaluation of settlements in sand deposits following liquefaction during earthquakes. Soils and foundations 32 (1), 173-188. *https://doi.org/10.3208/sandf1972.32.173*

Kokusho, T., 1999. Water film in liquefied sand and its effect on lateral spread. Journal of Geotechnical and Geo-Environmental Engineering 125 (10), 817-826. *https://doi.org/10.1061/(ASCE)1090-0241(1999)125:10(817)*

Kumar, R., Horikoshi, K., Takahashi, A., 2019. Centrifuge testing to investigate effects of partial

saturation on the response of shallow foundation in liquefiable ground under strong sequential ground motions. Soil Dynamics and Earthquake Engineering, 125, 105728. *https://doi.org/10.1016/j.soildyn.2019.105728*

Kutter B. L., 2013. Effects of capillary number, Bond number, and gas solubility on water saturation of sand specimens. Can Geotech J. 50 (2), 133–144. *https://doi.org/10.1139/cgj-2011-0250.*

Liu, L., Dobry, R., 1997. Seismic response of shallow foundation on liquefiable sand. Journal of geotechnical and geoenvironmental engineering 123 (6), 557-567. *https://doi.org/10.1061/(ASCE)1090-0241(1997)123:6(557)*

Mitchell, J. K., 1981. Soil improvement-state of the art report. In Proc., 11th Int. Conf. on SMFE 4, 509-565.

Mitchell, J. K., Baxter, C. D., Munson, T. C., 1995. Performance of improved ground during earthquakes. In Soil improvement for earthquake hazard mitigation, 1-36.

Nakai, S., Sekiguchi, T., 2011. Damage due to liquefaction during the 2011 Tohoku earthquake. In Proc. of the International Symposium for CSMID, 1-8.

Olarte, J., Paramasivam, B., Dashti, S., Liel, A., Zannin, J., 2017. Centrifuge modeling of mitigation-soil-foundation-structure interaction on liquefiable ground. Soil Dynamics and Earthquake Engineering 97 (4), 304-323. *https://doi.org/10.1016/j.soildyn.2017.03.014*

Priebe, H. J., 1989. The prevention of liquefaction by vibro replacement. In Proceedings of the 2nd International Conference on Earthquake Resistant Construction and Design, 211-219.

Sancio, R., Bray, J. D., Durgunoglu, T., Onalp, A., 2004. Performance of buildings over liquefiable ground in Adapazari, Turkey. In Proc., 13th World Conf. on Earthquake Engineering. Vancouver, Canada: Canadian Association for Earthquake Engineering.

Schaefer, V. R., Abramson, L. W., Drumheller, J. C., Sharp, K. D., 1997. Ground improvement, ground reinforcement and ground treatment: Developments, 1987-1997.

Schofield, A. N., 1981. Dynamic and earthquake geotechnical centrifuge modelling.

Seed, H. B., and Booker, J. R., 1977. Stabilization of potentially liquefiable sand deposits using gravel drains. Journal of Geotechnical and Geo-Environmental Engineering 103.

Shamoto, Y., Zhang, J. M., Tokimatsu, K., 1998. Methods for evaluating residual post-liquefaction ground settlement and horizontal displacement. Soils and Foundations, 38, 69-83. *https://doi.org/10.3208/sandf.38.Special_69*

Takemura, J., Kondoh, M., Esaki, T., Kouda, M., Kusakabe, O., 1999. Centrifuge model tests on double propped wall excavation in soft clay. Soils and Foundations,39 (3), 75-87. *https://doi.org/10.3208/sandf.39.3_75*

Tokimatsu, K., Katsumata, K., 2012. Liquefaction-induced damage to buildings in Urayasu city during the 2011 Tohoku Pacific earthquake. In Proceedings of the International Symposium on Engineering Lessons Learned from the 2011 Great East Japan Earthquake, 665-674.

Tokimatsu, K., Seed, H. B., 1987. Evaluation of settlements in sands due to earthquake shaking. Journal of Geotechnical Engineering 113 (8), 861-878. *https://doi.org/10.1061/(ASCE)0733-9410(1987)113:8(861)*

Yamaguchi, A., Mori, T., Kazama, M., Yoshida, N., 2012. Liquefaction in Tohoku district during the

2011 off the Pacific Coast of Tohoku Earthquake. Soils and Foundations 52 (5), 811-829. *https://doi.org/10.1016/j.sandf.2012.11.005*

Yoshimi, Y., 1977. Settlement of building on saturated sand during earthquake. Soils and Found 17 (1).

Zeybek A., Madabhushi S. P. G., 2017. Influence of air injection on the liquefaction-induced deformation mechanisms beneath shallow foundations. Soil Dynamics and Earthquake Engineering 97, 266-276. *https://doi.org/10.1016/j.soildyn.2017.03.018*

Zhang, J. M., Wang, G., 2012. Large post-liquefaction deformation of sand, part I: physical mechanism, constitutive description and numerical algorithm. Acta Geotechnica 7 (2), 69-113. *https://doi.org/10.1007/s11440-011-0150-7*

Table 1. Scaling law for centrifuge test (Schofield, 1981)

Parameters	Ratio of model to prototype
Length	1/N
Area	$1/N^2$
Volume	$1/N^3$
Acceleration	N
Stress	1
Strain	1
Time (dynamic)	1/N
Force	$1/N^2$
Bending moment	$1/N^3$

Table 2. Configuration of model foundation and superstructure

Property	Model foundation and superstructure*	
	Buffer Tank	Flare Stack
Footing dimension	4 x 4 x 1 m^3	4 x 4 x 2 m^3
Material used	Aluminum	Aluminum
Mass of footing	44.8 ton	87.04 ton
Thickness of superstructure	6 cm	6 cm
Outer diameter of superstructure	1.6 m	1.6 m
Height of lumped mass	7.6 m	14 m
Flexural rigidity (*EI*) of the superstructure	3.15 x 10^6 kN-m^2	3.15 x 10^6 kN-m^2
Lumped mass	28.16 ton	14.08 ton
Bearing pressure @ 40g	51.2 kPa	71.2 kPa
Design period of foundation-structure system	0.4s (2.5 Hz)	0.5s (2.0 Hz)

*All units are given in prototype scale

Table 3. Index properties of Toyoura sand and Silica no. 3 and properties of friction pile

Description	Toyoura sand	Silica no. 3	Description	Friction pile (prototype)
Specific gravity, G_s	2.65	2.63	Material	SUS304
D_{50} (mm)	0.19	1.72	Length	10 m
D_{10} (mm)	0.14	1.37	Pile outer diameter	16 cm
Maximum void ratio, e_{max}	0.973	1.009	Pile inner diameter	12 cm
Minimum void ratio, e_{min}	0.609	0.697	Length (spiral blades)	2 m
Permeability, *k (m/s)*	2×10^{-4}	6.6×10^{-3}	Thickness (spiral blades)	2 cm
Relative density (approx..), D_r	50 %	30 %	Pile outer diameter (with spiral blades)	32 cm
			EI at Pile head	4.178×10^3 kN-m^2
			EA at Pile head	1.671×10^6 kN

Table 4. Locations of different transducers within the model grounds

Level	Transducers*	Location** (prototype scale)		Initial vertical effective stress (σ'_{vo}) at different levels***	
		X m	Z (depth) m	Magnitude, kPa (prototype scale)	Description
Level 1	P1, A1	12	10	102.40	Model centerline
Level 2	A2	12	8	73.92	Model centerline
Level 3	P2	18	6	61.22	Below FS footing
	P3, A3	12	6	65.44	Model centerline
	P4	6	6	57.52	Below BT footing
Level 4	P5	18	4	54.49	Below FS footing
	P6, A4	12	4	41.96	Model centerline
	P7	6	4	47.49	Below BT footing
Level 5	P8	18	2	53.80	Below FS footing
	P9, A5	12	2	26.16	Model centerline
	P10	6	2	41.80	Below BT footing

* P: Pore water pressure transducers, A: Accelerometers

**Locations of the transducers are identical in all the models (Models 1-6)

*** Including vertical stress induced by the foundation-structure systems

Table 5. Test description and relative density and degree of saturation (at 1g) for Models 1-6

Test code	Model description	Relative density	Degree of saturation
Model 1	LG: Liquefiable ground	D_r = *52.8 %*	99.4 %
Model 2	LG-GD1: Liquefiable ground with gravel drainage type 1*	D_r = *51.6 %*	99.2 %
Model 3	LG-GD2: Liquefiable ground with gravel drainage type 2**	D_r = *54.0 %*	99.5 %
Model 4	LG-FP: Liquefiable ground with friction piles	D_r = *53.1 %*	99.1 %
Model 5	LG-GD1_FP: Liquefiable ground with gravel drainage type 1 and friction piles	D_r = *53.9 %*	99.3 %
Model 6	LG-GD2_FP: Liquefiable ground with gravel drainage type 2 and friction piles	D_r = *55.2 %*	99.2 %

*Gravel drainage type 1: Group of 5 x 5 gravel drains with 0.4 m diameter of each drain and 0.7 m clear spacing

** Gravel drainage type 2: Group of 5 x 5 gravel drains with 0.6 m diameter of each drain and 0.6 m clear spacing

Table 6. Design specifications of gravel drainage Types 1 and 2

Specifications*	Gravel drainage Type 1	Gravel drainage Type 2
Drain diameter (m)	0.40	0.60
Length of gravel drain (m)	5.60	5.60
Clear spacing (m)	0.70	0.55
Treated Plan	4.8 m X 4.8 m	5.2 m X 5.2 m
Replacement area (%)	13.63	26.14
Maximum allowable clear spacing between gravel drains for target r_u = 0.7		
Earthquake intensity	For gravel drainage Type 1	For gravel drainage Type 2
Small EQ (Neq/NL = 1) **	0.74 m	1.12 m
Medium EQ (Neq/NL = 2) **	0.44 m	0.80 m
Strong EQ (Neq/NL = 3) **	0.28 m	0.64 m

* The layout of both gravel drainage types are shown in Fig. 1

** For more details, readers are suggested to read Seed and Booker (1977) and Bouckovalas et al. (2009)

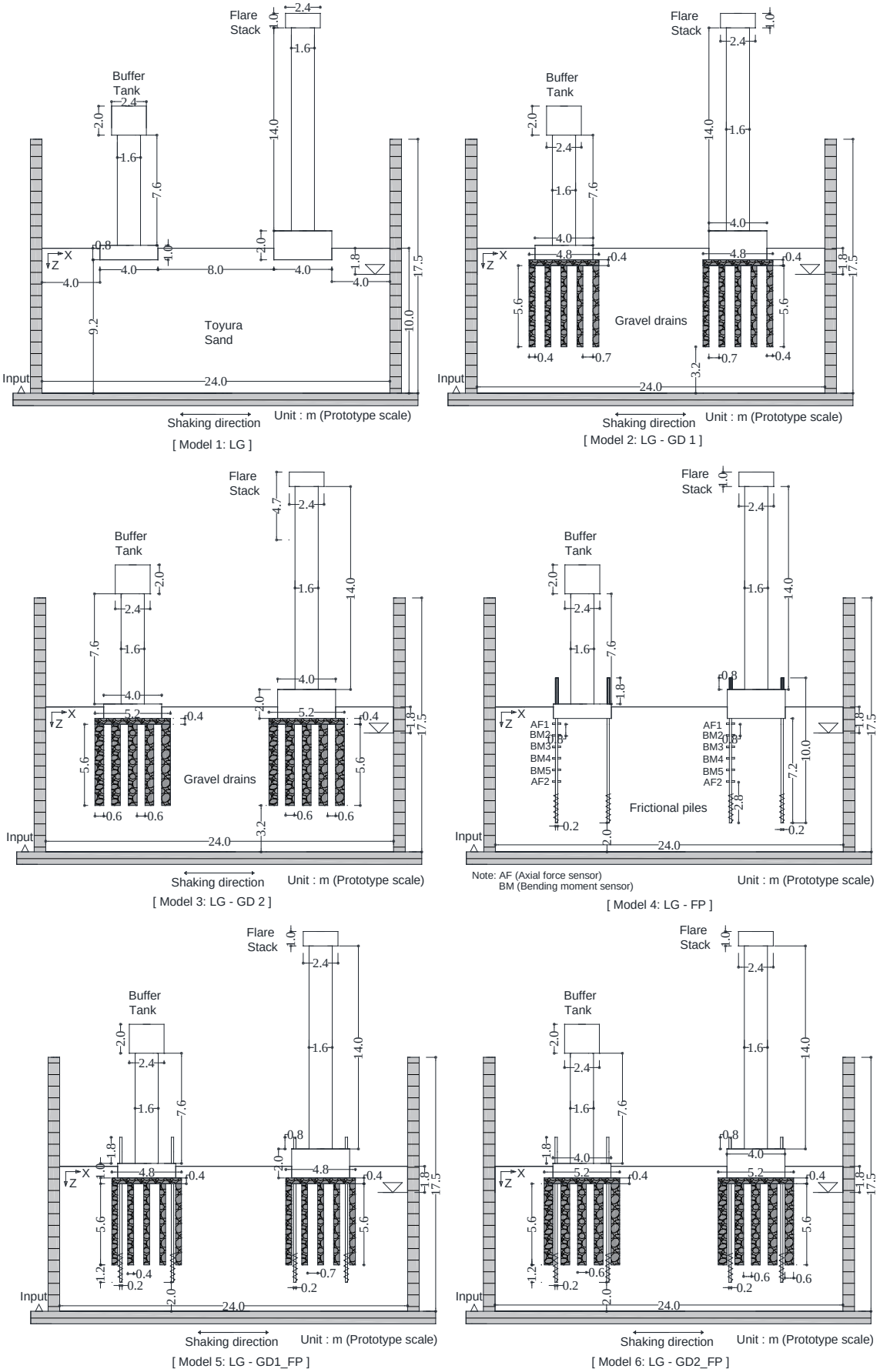

Figure 1. Models configuration in prototype scale

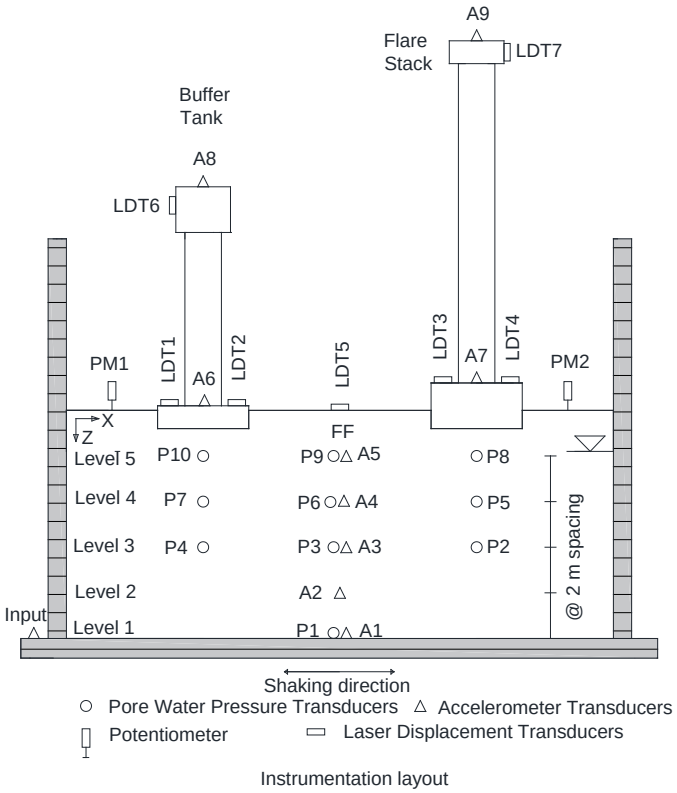

Figure 2. Different transducers layout in centrifuge model

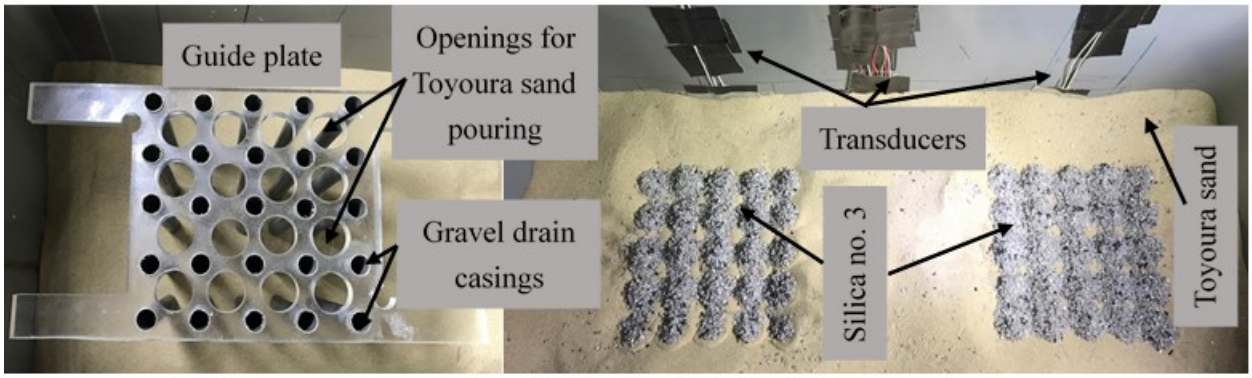

Figure 3. Guide plate to form the gravel drains and the typical array of gravel drains after removing the guide plates (for both BT and FS)

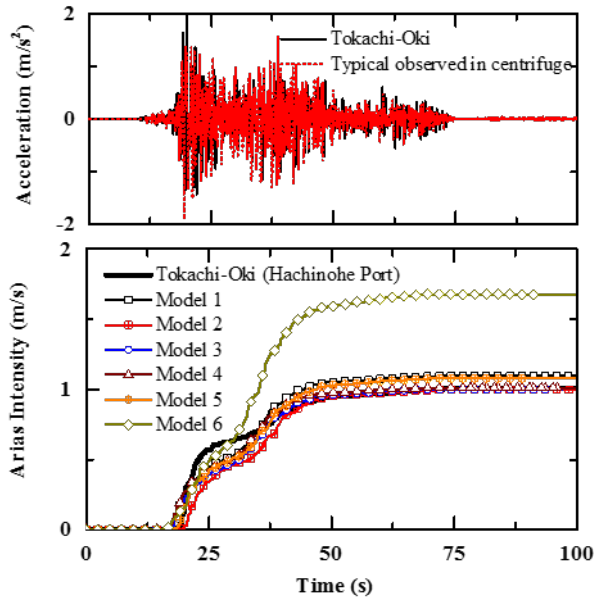

Figure 4. Typical observed acceleration time history in centrifuge and Arias intensities of all Models 1-6 for input Tokachi-Oki ground motion.

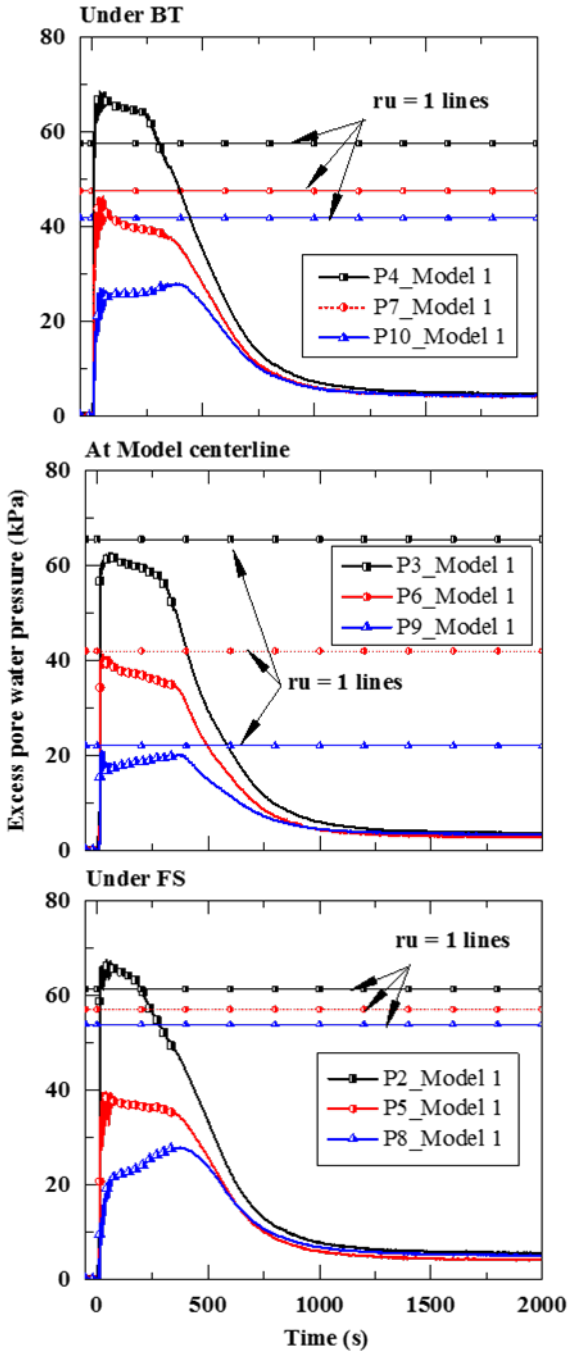

Figure 5. Excess pore water pressure time histories of Model 1 during Tokachi-Oki ground motion

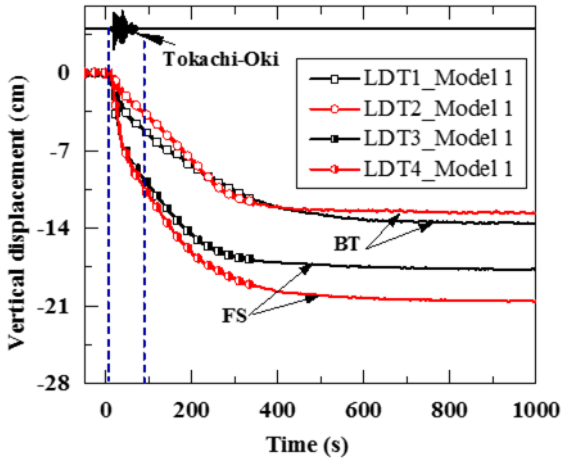

Figure 6. Settlement time histories of BT (LDT1 & 2) and FS (LDT3 & 4) of Model 1 during Tokachi-Oki ground motion

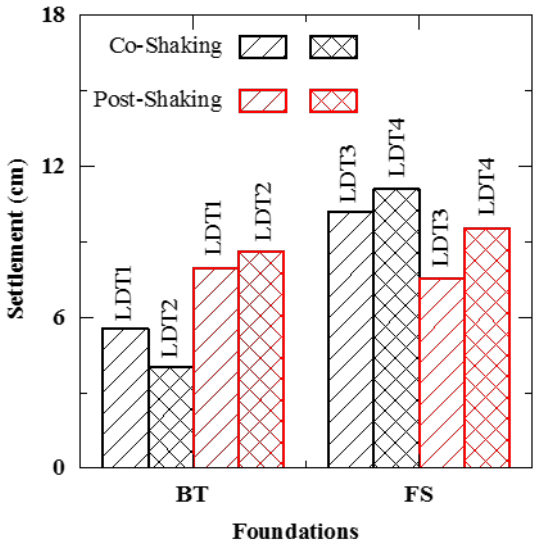

Figure 7. Co-shaking and post-shaking settlement of BT (LDT1 & 2) and FS (LDT3 & 4) for Model 1

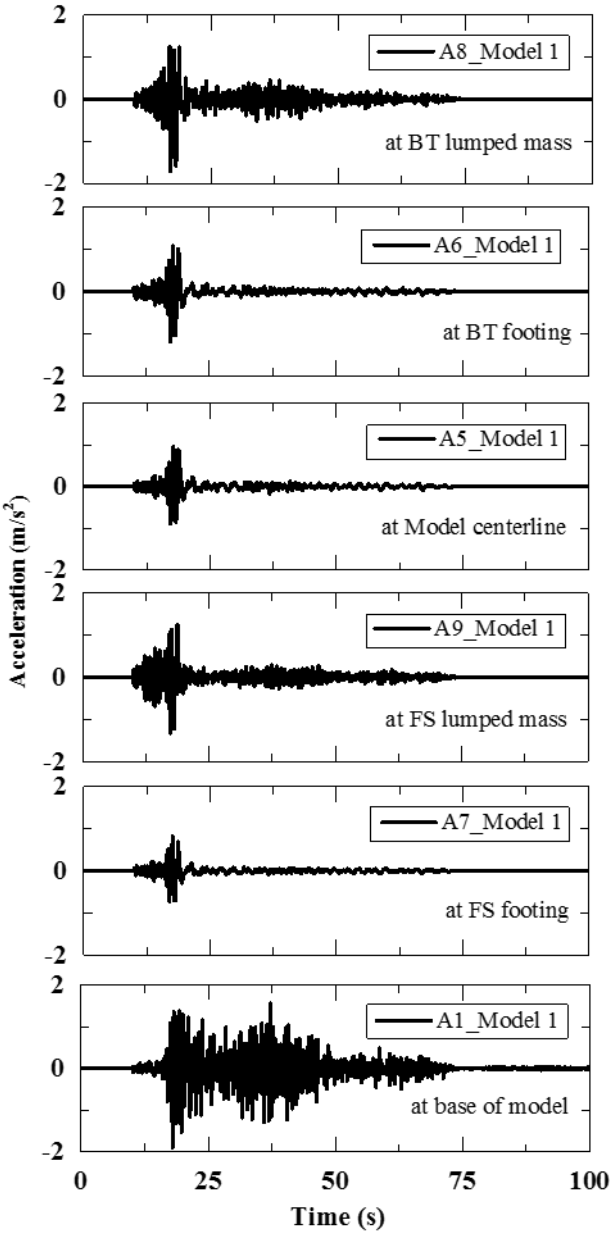

Figure 8. Acceleration response of Model 1 during Tokachi-Oki ground motion

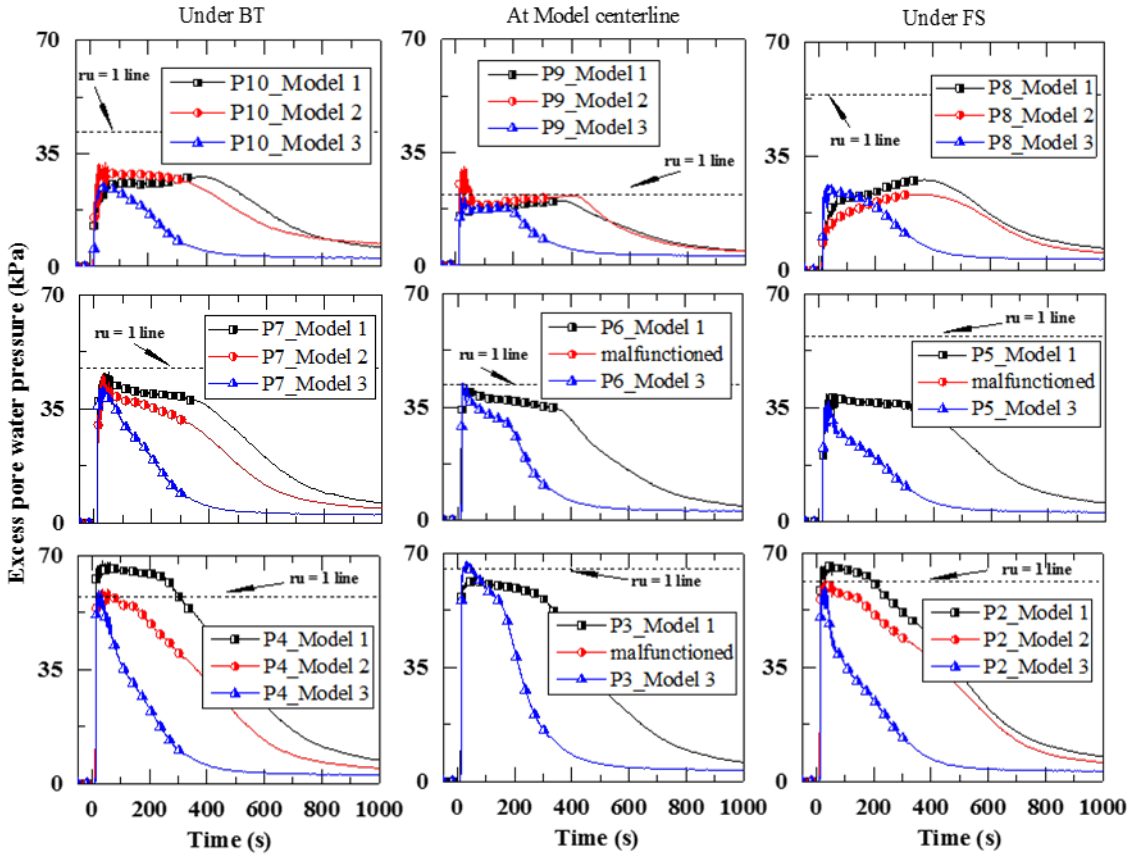

Figure 9. Excess pore water pressure time histories of Models 1-3 during Tokachi-Oki ground motion

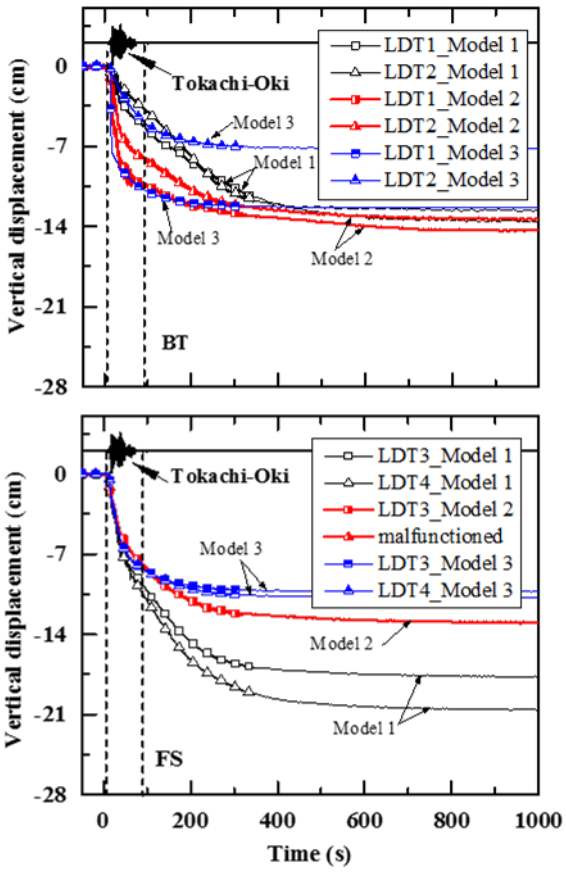

Figure 10. Settlement time histories of BT (LDT1 & 2) and FS (LDT3 & 4) of Models 1-3 during Tokachi-Oki ground motion

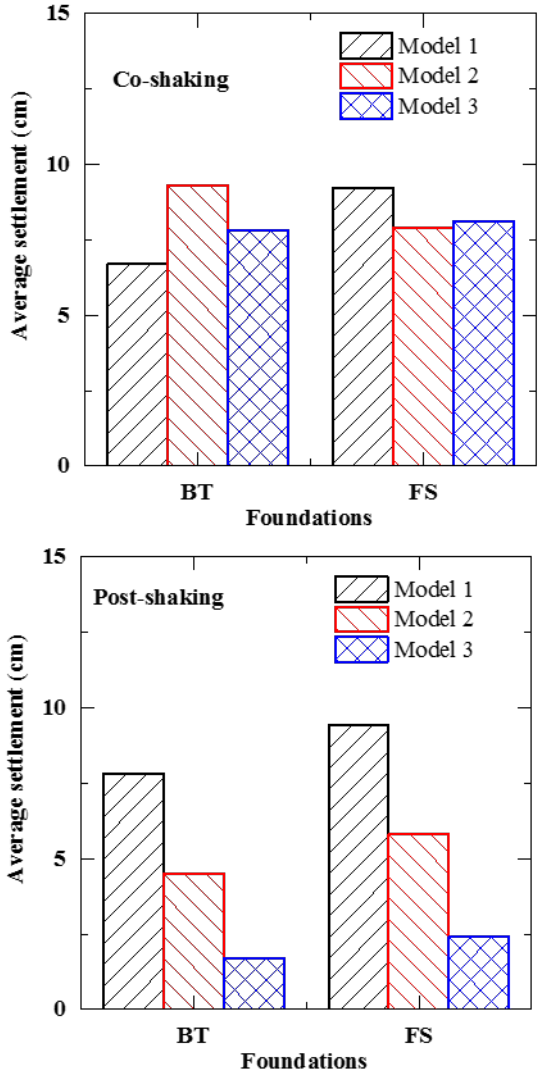

Figure 11. Average settlement during co-shaking and post-shaking phase for Models 1-3

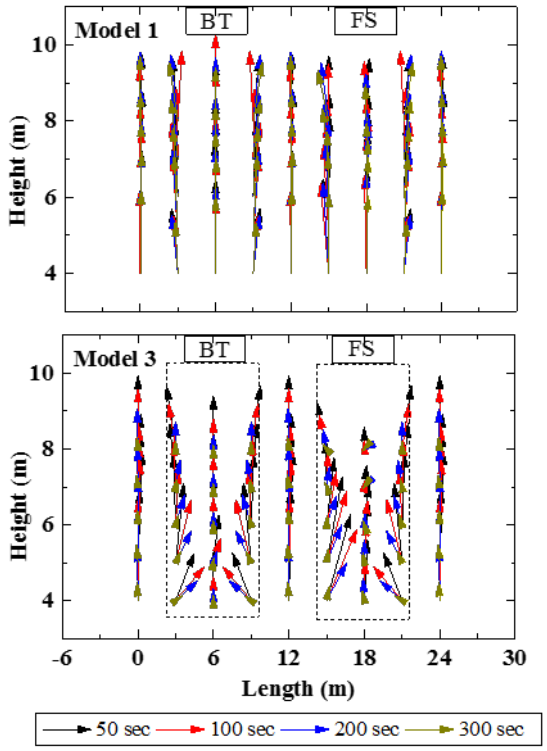

Figure 12. Pore fluid flow at different times for Models 1 and 3 during Tokachi-Oki ground motion

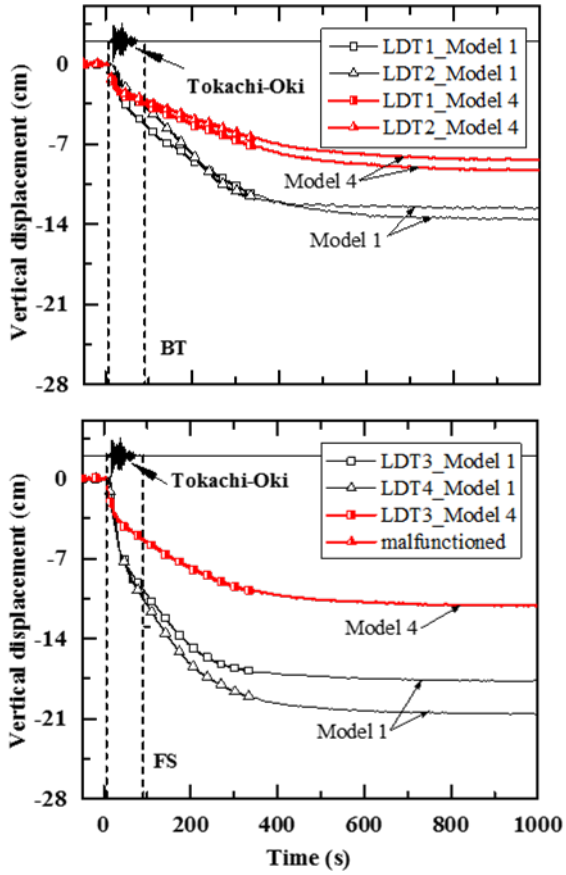

Figure 13. Settlement time histories of BT (LDT1 & 2) and FS (LDT3 & 4) of Models 1 and 4 during Tokachi-Oki ground motion

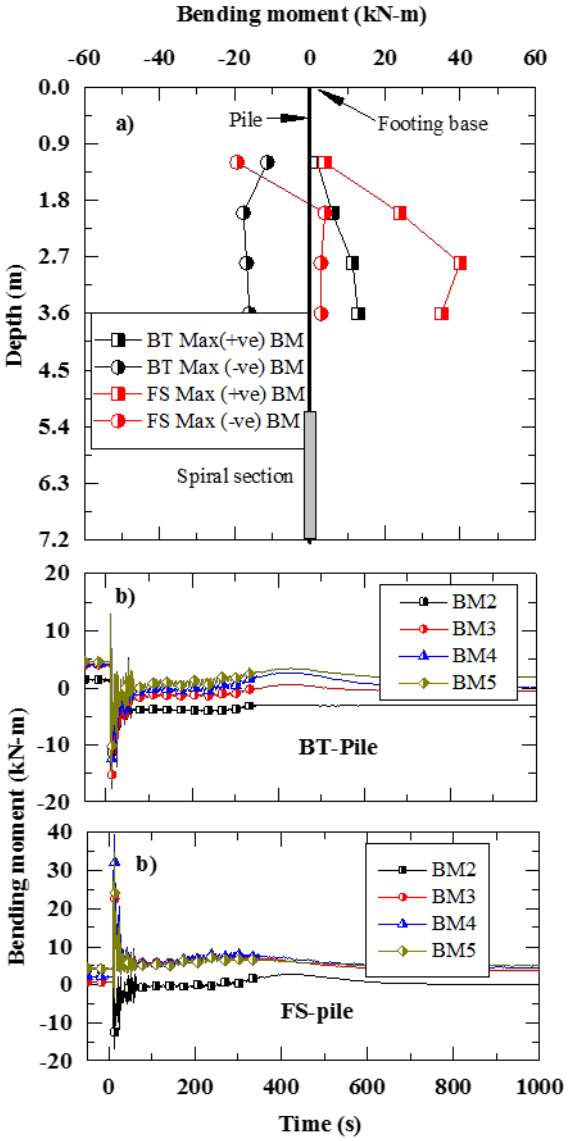

Figure 14. Exerted bending moment on friction piles a) bending moment envelope, and b) bending moment time histories during Tokachi-Oki ground motion

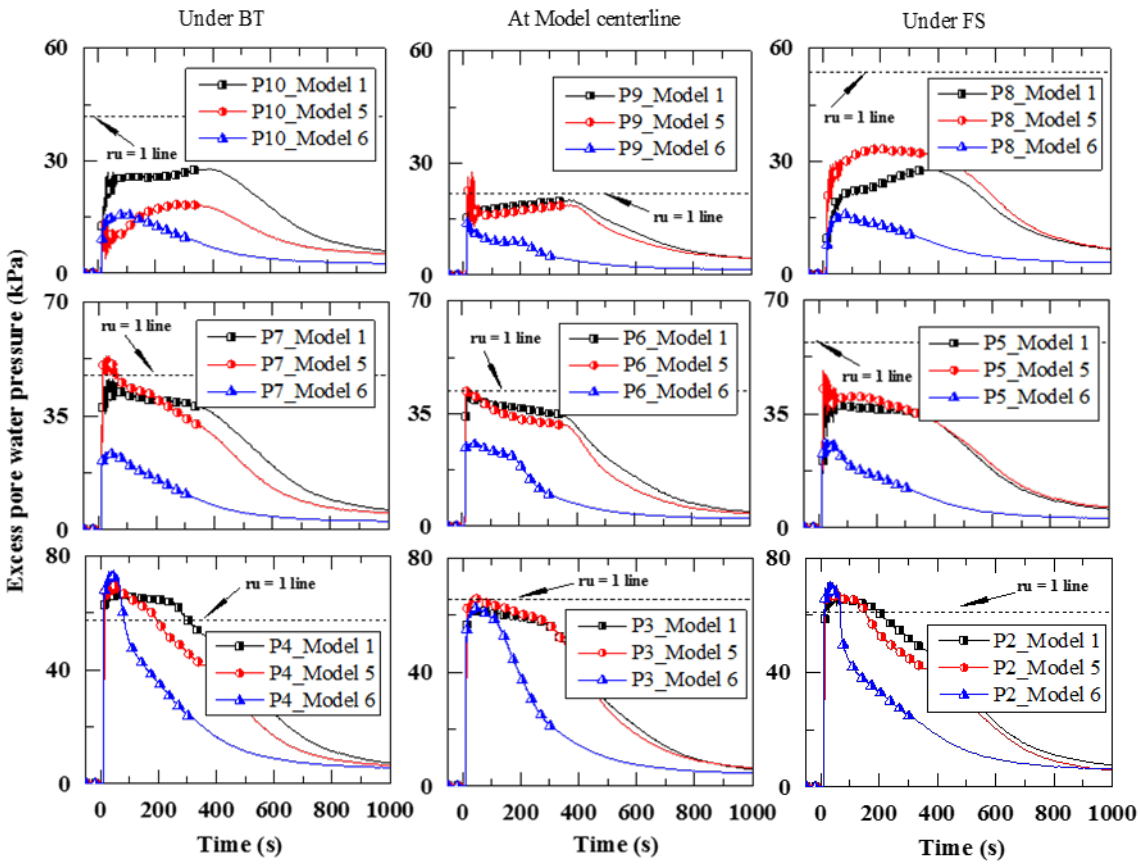

Figure 15. Excess pore water pressure time histories of Models 1, 5 and 6 during Tokachi-Oki ground motion

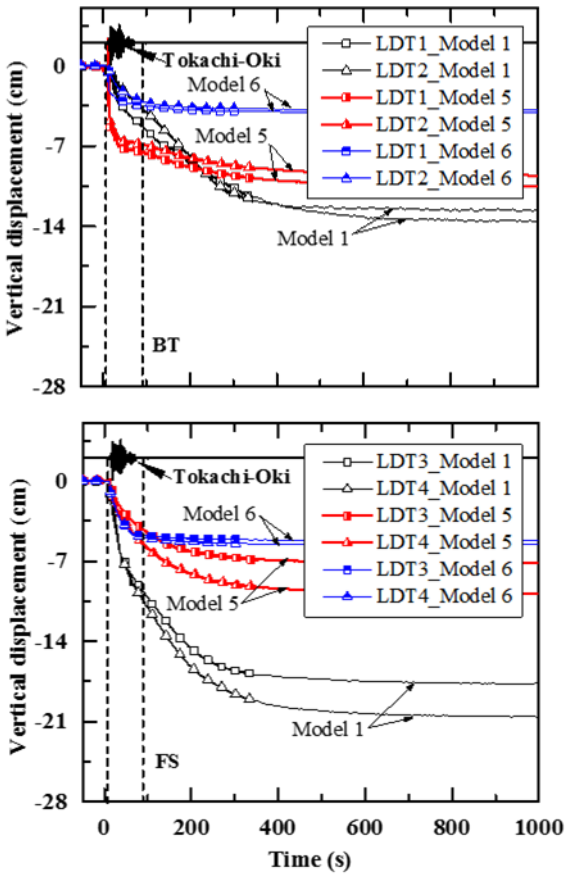

Figure 16. Settlement time histories of BT (LDT1 & 2) and FS (LDT3 & 4) of Models 1, 5 and 6 during Tokachi-Oki ground motion

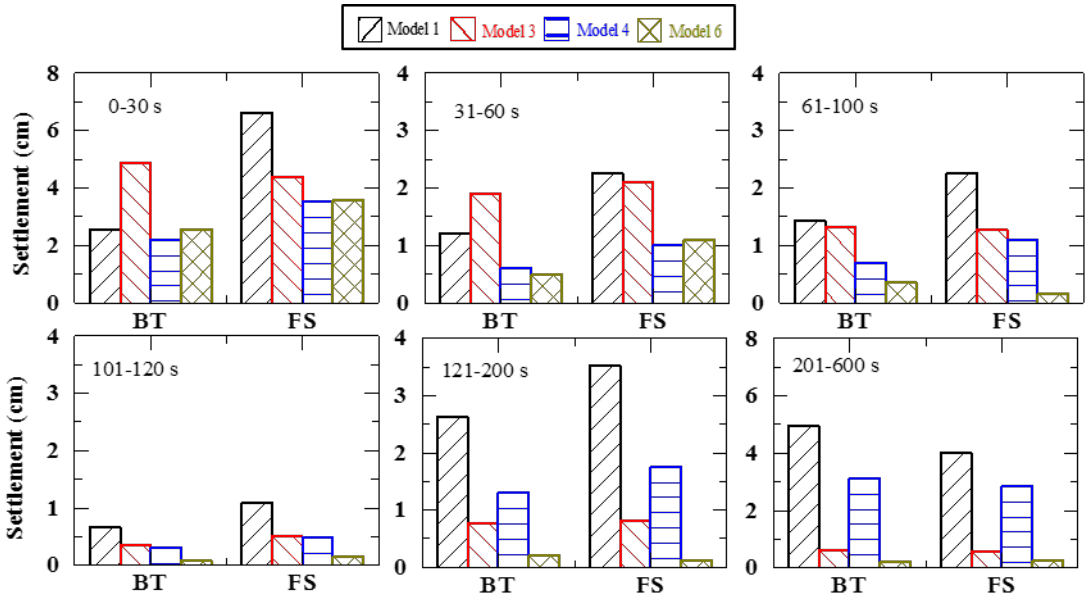

Figure 17. Average settlement of BT and FS footings for different time periods during Tokachi-Oki ground motion